Analyst

Accepted Manuscript

ROYAL SOCIETY OF CHEMISTRY

www.rsc.org/analyst

Aptasensor based on tripetalous cadmium sulfide-graphene electrochemiluminescence for the detection of carcinoembryonic antigen

Gui-Fang Shi,[a] Jun-Tao Cao,[a] Jing-Jing Zhang,[a] Ke-Jing Huang,[a] Yan-Ming Liu,[a,*] Yong-Hong Chen[b], Shu-Wei Ren[b]

[a]*College of Chemistry and Chemical Engineering, Xinyang Normal University, Xinyang 464000, China,*

[b]*Xinyang Central Hospital, Xinyang 464000, China*

*To whom correspondence should be addressed. E-mail: liuym9518@sina.com.

Tel & Fax: +86-376-6392889.

Abstract

A facile label-free electrochemiluminescence (ECL) aptasensor based on the ECL of cadmium sulfide-graphene (CdS-GR) nanocomposites with peroxydisulfate as coreactant was designed for the detection of carcinoembryonic antigen (CEA). Tripetalous CdS-GR nanocomposites were synthesized through a simple onepot solvothermal method and immobilized on the glassy carbon electrode surface. L-cystine (L-cys) could promote the electron transfer and enhance the ECL intensity largely. Gold nanoparticles (AuNPs) were assembled onto the L-cys film modified electrode to the aptamer immobilization and the ECL signal amplification. The aptamer modified with thiol was adsorbed onto the AuNPs surface through Au-S bond. Upon the hybridization of the aptamer with target protein, the sequence could conjugate CEA to form Y architecture. With the CEA as a model analyte, the decreased ECL intensity is proportional to CEA concentration in the range of 0.01 - 10.0 ng/mL with the detection limit of 3.8 pg/mL (*S/N* = 3). The prepared aptasensor has been applied to determination of CEA in human serum samples. The recoveries of CEA in human serum samples are between 85.0% and 109.5%, and the RSD values are no more than 3.4%.

Keywords: electrochemiluminescence, aptasensor, tripetalous CdS-Graphene composites, carcinoembryonic antigen, gold nanoparticles

1. Introduction

Aptamers are artificially synthesized nucleic acids, having the advantages of simple synthesis, good stability, easily chemical modification and wide applicability to extreme conditions.[1] They are also attractive recognition elements due to their ability of high specificity and affinity to bind with target proteins. Carcinoembryonic antigen (CEA) is a 180 kDa glycoprotein belonging to the immunoglobulin superfamily[2] and its aptamer has been reported.[3,4] And it is most often associated with colorectal carcinomas and commonly used as a clinical tumor marker for clinical diagnosis of colon tumors, breast tumors, ovarian carcinoma and cervical carcinomas. Usually, the content of CEA in biological samples is very low and the cut-off values for CEA in human serum is 5 ng/mL.[5] Hence, the sensitive determination of CEA is very important in clinical tumor diagnoses and prognosis of original carcinoma. The common technique used for the determination of CEA is immunoassay, such as square wave voltammetry,[6] differential pulse voltammetry,[7] electrochemiluminescence (ECL),[8] fluorescence[9] and capillary electrophoresis-chemiluminescence.[10] Recently, aptamer-based detection methods have been developed. For example, Zeng *et al.*[4] constructed a signal-on photoelectrochemical aptasensor with a detection limit of 0.47 pg/mL. Zhou *et al.*[11] reported aptamer-based fluorescence-coupled affinity probe capillary electrophoresis technique for analysis of CEA with the detection limit of 5 pg/mL (S/N = 3). Lin *et al.*[12] designed a fluorescence biosensor for CEA detection in the range of 0.1 - 10 ng/mL. Shu *et al.*[13] developed an electrochemical aptasensor by

differential pulse voltammetry to quantify the concentration of CEA with a detection limit of 0.5 ng/mL.

ECL is a form of chemiluminescence in which the light emitting chemiluminescent reaction is preceded by an electrochemical reaction. ECL shows many advantages, including high versatility, simple optical setup, good temporal and spatial control and very low background signal.[14] ECL of luminol, quantum dots, tris (2, 2'-bipyridyl) ruthenium (II) and their analogs have been documented.[15] Since Bard *et al.*[16] explored ECL properties of silicon semiconductor nanocrystals in 2002, the preparation and application of various ECL semiconductor nanocrystals including CdS,[17] CdSe,[18] and CdTe,[19] has received extensive research attention. Some new nanostructures have been developed to improve the ECL intensity and biocompatibility, such as CdS composites with carbon nanotubes,[20] TiO_2,[21] graphene oxide (GO)[22] and GR.[23] GR has been successfully used as biocompatible interfaces due to its high specific surface areas, excellent electronic conductivity, and good biocompatibility.[24] It has been found that the CdS-GR composites could enhance the surface areas and facilitate the electrochemical redox process of CdS.[25] Recently, morphology-controlled synthesis and self-assembly of nanoscale building blocks into three-dimensional (3D) complex architectures have been a research hot spot.[26] The preparation of CdS-GR usually using dimethyl sulfoxide as the precursor for sulfide, and the solvent would result in large amounts of sulfur-containing organic waste and is not environmentally friendly.[27] So a facile, one-step, environmentally benign method for the synthesis of

CdS-GR composites with 3D structure is necessary.

Recently, several investigations focused on improving ECL signals in an attempt to obtain higher sensitivity.[28] AuNPs are an effective platform for the fabrication of label-free sensors due to the merits of high surface reactivity, excellent biocompatibility, and good catalytic activity.[29,30] L-cysteine (L-cys) film has advantages like controllable, compact, stable, and favorable for electron transfer toward the electrode surface. It has been reported that both AuNPs and L-cys have a great enhancement to the ECL intensity of peroxydisulfate ($S_2O_8^{2-}$).[31] $S_2O_8^{2-}$ is one of the most commom coreactant in the ECL systems and it could be electrochemically reduced to sulfate radical anion ($SO_4^{\cdot-}$), a strongly oxidizing intermediate.[32] The principle of ECL could be described as follows:

$$\text{CdS-GR} + e^- \rightarrow \text{CdS-GR}^{\cdot-} \quad (1)$$

$$S_2O_8^{2-} + e^- \rightarrow SO_4^{2-} + SO_4^{\cdot-} \quad (2)$$

$$\text{CdS-GR}^{\cdot-} + SO_4^{\cdot-} \rightarrow \text{CdS-GR}^* + SO_4^{2-} \quad (3)$$

$$\text{CdS-GR}^* \rightarrow \text{CdS-GR} + h\nu \quad (4)$$

Herein, we prepared 3D structure CdS-GR nanocomposites via one-step hydrothermal method. A novel ECL aptasensor for sensitive and specific detection of CEA targets with CdS-GR as ECL luminophores, L-cys and AuNPs as amplification regents was constructed. The positive charged L-cys film was assembled on the negative charged nafion film and sulfhydryl of L-cys could covalently interact with AuNPs through Au-S bond. Thus, the ECL intensity was amplified and the detection

sensitivity was further enhanced largely. The process of the stepwise modification of GCE was investigated in detail. The prepared aptasensor was successfully applied to the determination of CEA in human serum samples.

2. Experimental

2.1 Reagents

The CEA binding aptamer (5'-SH-TTT TTT ATA CCA GCT TAT TCA ATT-3') was synthesized by Sangon Biotech Co., Ltd. (Shanghai, China). $HAuCl_4 \cdot 3H_2O$ was purchased from Alfa Aesar (Tianjin, China). Citric acid trisodium salt dihydrate ($C_6H_5Na_3O_7 \cdot 2H_2O$) was from the Sinopharm Group Chemical Reagent Co., Ltd. (Shanghai, China). Polyvinylpyrrolidone (PVP), human serum albumin (HSA), human IgG (hIgG), human IgE (hIgE) and bovine serum albumin (BSA, Mr = 67000) were from Shanghai Solarbio Bioscience & Technology Co., Ltd. (Seebio Biotechnology). Nafion (5 wt%) was from Sigma-Aldrich (USA). Graphite powder, $CdCl_2$, thiourea and L-cys were from Shanghai Chemical Reagent Corporation (Shanghai, China). CEA was donated by Ms Yan-Li Zheng from Zhengzhou Immuno Biotech Co., Ltd. (Zhengzhou, China).

0.2 M phosphate buffer saline (PBS, pH 7.4) from Sangon Biotech Co., Ltd. (Shanghai, China) was used to dissolve aptamer and CEA. All chemicals were of analytical grade. The water used throughout the experiments was processed with an Ultrapure Water System (Kangning Water Treatment Solution Provider, China).

2.2 Apparatus

Cyclic voltammetry (CV) and electrochemical impedance spectroscopy (EIS) measurements were carried out with RST5200F electrochemical workstation (Zhengzhou Shiruisi Technology Co., Ltd., China). A three-electrode system was composed of a modified glassy carbon electrode (GCE, φ = 3 mm) as the working electrode, a Pt spiral wire as the counter electrode and an Ag/AgCl as the reference electrode. EIS measurements were carried out in 5.0 mM $K_3Fe(CN)_6/K_4Fe(CN)_6$ (1:1) containing 0.1 M KCl. Scanning electron microscopy (SEM) images were obtained by S-4800 (Hitachi, Tokyo, Japan). The high resolution transmission electron microscopy (HRTEM) images were recorded with Tecnai G^2 F20 TEM system (FEI Co., America). X-ray powder diffraction (XRD) pattern was operated on Rigaku-Mini Flex 600 (Tokyo, Japan). Fourier transform infrared (FT-IR) spectrum was recorded on Bruker TENZOR 27 spectrophotometer (Germany). Raman spectra were collected by using the Renishaw InVia Raman microscope (UK), excited with excitation laser wavelength of 532 nm at room temperature.

2.3 Preparation of CdS-GR

The GO was synthesized from graphite flake using the Hummers' method.[33] The CdS-GR nanocomposites were synthesized via a hydrothermal process of modified Gao's work.[34] Briefly, 1.6 g GO was ultrasonically dispersed in 80 mL ethylene glycol to obtain a clear GO dispersion. 1.54 g $CdCl_2$ was added to the dispersion and stirred

for 1 h. Then 0.64 g of thiourea and 0.96 g of PVP were added to the GO dispersion under stirring to afford a transparent mixture. Subsequently the dispersion was transferred to a Teflon-lined stainless steel autoclave which was heated to 100 ºC for 24 h. After cooling naturally, the black precipitates was collected by centrifugation, washed with water and ethanol, and dried in a vacuum oven at 80 ºC overnight to obtain CdS-GR composites. Pure CdS was also synthesized by the same procedure but no GO.

2.4 Preparation of AuNPs

The preparation of AuNPs followed Frens' method.[35] Briefly, 50 mL 0.01% (w/v) $HAuCl_4$ solution was brought to vigorous boiling with stirring. Then 0.6 mL 2.0% (w/v) trisodium citrate solution was added to the $HAuCl_4$ solution quickly. The colour of the solution changed from pale yellow to wine red in a few seconds. The mixture was maintained at the boiling point for 15 min and then cooled to room temperature under continuous stirring. The AuNPs with average size of 20 nm were synthesized and stored at 4 ºC.

2.5 Fabrication of the ECL aptasensor

The self-assembly procedure of fabrication of the aptasensor was illustrated in Scheme 1. GCE was carefully polished with 0.3 and 0.05 μm alumina powder sequentially, rinsed with ethanol and water, and then dried under ambient nitrogen gas. Firstly, the GCE was modified by drop-coating of 5 μL of 1 mg/mL CdS-GR

suspension. Secondly, 10 μL of 0.1 wt% nafion solution was dropt onto the GCE and dried in the air. Then the modified GCE was immersed into L-cys solution (pH = 3) for 6 h. After that, 10 μL AuNPs were modified on the electrode for 3 h. Subsequently, the resultant electrode was immersed into 1.0 μM aptamer solution for 12 h to form the aptasensor through strong Au-S bond. The unbonded aptamer was removed by washing the modified electrode with PBS. Finally, 10 μL 1 wt% BSA was dropped on the electrode for 1 h to block the non-specific binding sites of AuNPs and followed by washing with PBS and stored at 4 ℃ when not in use. The aptasensor was immersed into CEA solution at 37 ℃ for 2 h to detect target CEA.

Here Scheme 1

2.6 ECL Measurement

ECL intensity of the aptasensor was measured with a BPCL Ultra-weak luminescence analyzer (Institute of Biophysics, Chinese Academy of Science, Beijing, China) with a CR 120 type photomultiplier tube (Binsong Photonics, Beijing, China). CV mode with continuous potential scanning from 0 to -1.6 V and scanning rate of 100 mV s^{-1} were used to achieve ECL signal in 10 mL detection solution (0.1 M PBS containing 0.1 M $K_2S_2O_8$). The 0.1 M PBS was prepared by mixing stock solutions of NaH_2PO_4 and Na_2HPO_4 and then adjusting to the desired pH using NaOH and H_3PO_4. The ECL and CV curves were recorded simultaneously.

3. Results and discussion

3.1 Characterization of materials

SEM images in Fig. 1 show the surface morphologies of GO (Fig. 1A), GR (Fig. 1B), CdS (Fig. 1C), and CdS-GR (Fig. 1D) composites, respectively. From Fig. 1A and Fig. 1B, it can be seen that the sheets of GO and GR are thin. The images in Fig. 1C reveal that the CdS particles possess three petal-like structures and are very uniform about 200 nm in size. Each petal has a cone-like shape, and the assembly of three petals into this kind of geometry retains the large surface area of these anisotropic petal units. The images of CdS-GR composites in Fig. 1D show that tripetalous CdS was attached onto the GR sheet.

Here Fig. 1

The morphology and structure of these nanomaterials were further elucidated by TEM, as shown in Figure 2. Single layered GR (Fig. 2A) shows transparent two-dimensional sheets structure and the sheets of GR are thin. From Fig. 2B, it can be seen that CdS nanospheres are uniformly distributed with tripetalous structure. Notably, using of ethylene glycol (EG) and PVP as the solvent and shape modifier respectively is critical for the formation of dispersed uniform petalous particles.[36] As for CdS-GR composites (Fig. 2C), the tripetalous CdS composites are uniformly distributed on layered GR sheets.

Here Fig. 2

Raman scattering is an effective technique to investigate the crystallization, structure, and defect of the nanostructure materials. Fig. 3A shows a typical Raman

spectrum of GR, CdS, and CdS-GR composites, respectively. The Raman spectra of GR (curve a) and CdS-GR (curve b) hybrids display two prominent peaks at around 1580 cm^{-1} and 1340 cm^{-1}, corresponding to the G and D bands, respectively.[37] From curve b and c (CdS), both samples exhibit two Raman active peaks at about 295 cm^{-1} and 589 cm^{-1}, which are the characteristic LO phonon mode and two-phonon overtone of nanosized CdS materials, respectively. The results conform the formation of CdS-GR nanocomposites.

X-ray diffraction (XRD) measurements were performed to elucidate the crystalline phases of GO, GR, CdS and CdS-GR, as shown in Fig. 3B. The XRD pattern of pristine GO (curve a) shows a sharp peak at 9.13°, which corresponds to the (001) reflection of GO.[38] After reducing GO into GR (curve b), this peak disappeared. Meanwhile, it is easy to discovery that all the diffraction peaks for the CdS (curve c) could be well indexed to CdS phase (JCPDS: 01-089-0441). The XRD pattern of the GR-CdS composites (curve d) shows the peaks for the hexagonal CdS phase and the peak at 22.9° for GR, but no GO peaks were observed, indicating the formation of CdS and the reduction of GO.

Furthermore, the FTIR spectra of the GO (curve a), GR (curve b), CdS (curve c) and CdS-GR (curve d) composites were measured. As shown in Fig. 3C, the spectra of the GO (curve a) exhibits stretching vibrations of -OH (3423 cm^{-1}), -C=O (1720 cm^{-1}), C=C (1632 cm^{-1}), C-O (1225 cm^{-1}), and C-O-C (1059 cm^{-1}). The bending vibration of -OH in the carboxylic group was observed at 1400 cm^{-1}. After the solvothermal

reduction, as shown in curve b (GR) and curve d (CdS-GR), the C=C peak shifts from 1632 cm^{-1} to 1570 cm^{-1} which could be attributed to the π electrons interaction in the polarizable aromatic ring being transformed into cation-π interactions.[39] Furthermore, the stretching vibration of C=O has disappeared and other oxygen-containing functional groups in GO also decreased dramatically. For the CdS-GR (curve d), the double peaks at 2925 cm^{-1} and 2863 cm^{-1} correspond to the asymmetric and symmetric -CH_2- stretching, respectively. The presence of -CH_2- also confirms that GR has been functionalized with CdS during the reduction.

Here Fig. 3

3.2 Electrochemical and ECL behavior of the aptasensor

EIS is an effective method for probing the features of surface modified electrodes. The impedance spectra include semicircle portion and linear portion. The semicircle diameter at higher frequencies corresponds to the electron transfer resistance (R_{et}), and the linear part at lower frequencies corresponds to the diffusion process. The EIS behaviors of the step by step surface modification of the GCE in 5 mM $Fe(CN)_6^{4-/3-}$ (pH 7.4) containing 0.1 M KCl were shown in Fig. 4A. The semicircle the bare GCE in EIS is small (curve a), indicating that the charge transfer at bare electrode is relatively facile. After the electrode was modified with CdS-GR (curve b), the semicircles become large due to the low conductivity of CdS. When nafion (curve c) was dropt onto CdS-GR, the R_{et} value goes up. The reason is that nafion could act as the inert electron and mass transfer blocking layer, and it hinders the diffusion of

ferricyanide toward the electrode surface. As L-cys (curve d) was assembled, the R_{et} value decreased, certifying the positive charged L-cys could be absorbed into the nafion polymer via the ion exchanging effect. When AuNPs (curve e) was assembled, the semicircles become smaller which is attributed to the excellent conductivity of AuNPs. While the prepared electrode was combined with aptamer (curve f) and blocked with BSA (curve g) and incubated with CEA (curve h), the semicircles enlarged in succession were observed as the hindrance caused by aptamer, BSA and CEA, respectively.

In order to characterize the fabrication process of the ECL aptasensor, ECL signals at each immobilization step were recorded. As shown in Fig. 4B, the bare GCE (curve a) has weak ECL signal in the PBS containing $K_2S_2O_8$. When CdS-GR composite film was dropt on GCE, the ECL intensity enhanced greatly (curve b). The ECL intensity (curve c) decreased after nafion solution was dropt onto the electrode. Then the modified GCE was immersed into L-cys solution (curve d) and the ECL intensity was improved, which inferred that the L-cys plays a key role in the catalysis of ECL. After that, AuNPs colloids were assembled onto the electrode through Au-S bond, the ECL signal was further enhanced (curve e). The probable reason is that the AuNPs play an important role like a conducting wire, which makes it is easier for the electrons to transfer in ECL reaction. Finally, after aptamer (curve f) was immobilized onto the electrode and BSA (curve g) was used to block the nonspecific binding sites, the incubation with target protein (CEA, curve h), results in decreased ECL intensity

gradually. The reason is that the aptamer, BSA and CEA on the electrode acted as the inert electron and mass-transfer blocking layer, and hindered the diffusion of ECL reagents toward the electrode surface.

Here Fig. 4

3.3 Optimization of experimental conditions

The effect of the pH of the detection solution on the ECL intensity was investigated in the range of 6.4 - 7.8 (Fig. 5A). The ECL intensity increased from 6.4 to 7.0 and then decreased. The maximum ECL intensity was observed at pH 7.0. Since the optimal pH value for the biological systems is about 7.4, the pH 7.4 PBS was selected. The ionic strength is another parameter that affects the ECL intensity. The effect of KCl concentration of the supporting electrolyte over the range from 0.04 to 0.20 M was studied in the presence of $K_2S_2O_8$ (Fig. 5B). It can be found that the ECL intensity increased with increasing KCl concentration and reached the maximum value when KCl concentration is 0.1 M. So 0.1 M KCl was used.

Additionally, the concentration of $K_2S_2O_8$ has a profound impact on the ECL intensity (Fig. 5C). The ECL intensity increased gradually with increasing of $K_2S_2O_8$ concentration from 0.04 to 0.10 M and then decreased with further increasing of $K_2S_2O_8$ concentration. Thus, 0.10 M $K_2S_2O_8$ was chosen. The effect of the interaction time of CEA aptamer with CEA was investigated from 0.5 to 4 h. From Fig. 5D, the ECL intensity decreased with the increase of incubation time and reached a plateau at

2 h. Therefore, 2 h was selected.

Here Fig. 5

3.4 Analytical performance of the ECL aptasensor

Under the optimum conditions, the ECL aptasensor was used to detect CEA. Fig. 6A shows the ECL intensity of the aptasensor before (curve a) and after (curves b-k) reaction with different concentrations of CEA in the 10 mL 0.1 M PBS (pH 7.4) containing 0.1 M KCl and 0.1 M $K_2S_2O_8$. As can be seen, the ECL intensity in the presence of CEA (curve b) is lower than that in the absence of CEA (curve a), and the ECL intensity decreased gradually with increase of CEA concentration (curves b-k).

The change of ECL intensity ΔI has a linear relationship with the logarithm of CEA concentration in the range of 0.01 - 10.0 ng/mL (Fig. 6B), and the regression equation is $\Delta I = 39278 + 13958 \log C$ ($R = 0.997$). Where $\Delta I = I_0 - I$ (I_0 and I correspond to the ECL intensity of the before and after adding target protein), C is CEA concentration, and R is the regression coefficient. The detection limit of CEA was calculated to be 3.8 pg/mL ($S/N = 3$).

Here Fig. 6

3.5 Selectivity of the ECL aptasensor

The selectivity of the proposed aptasensor was examined by choosing HSA, hIgE, and hIgG as interferents and the results were shown in Fig. 7A. The concentrations of the HSA, hIgE, hIgG, and CEA were 40 mg/mL, 20 mg/mL, 20 mg/mL, and 1 ng/mL, respectively. The results shown that only CEA exhibits strong ΔI, while ΔI are of

only 3.5% for HSA, 3.9% for hIgE, and 3.0% for hIgG, respectively, compared with ΔI from CEA. The response of the aptasensor in a mixture of the above mentioned four proteins was also examined. The intensity of ΔI of the mixture had little difference with that in only CEA solution. These results indicate that the developed aptasensor has good selectivity for the detection of CEA.

The stability of the aptasensor (Fig. 7B) was tested by consecutive cyclic potential scans for 30 circles. The relative standard deviation (RSD) of ECL intensity was 1.5%. The repeatability of the aptasensor was also evaluated by analysis of the same concentration of CEA (1 ng/mL) using five aptasensors under the same conditions. The RSD of 5.2% was obtained.

Here Fig. 7

3.6 Application of the ECL aptasensor

To evaluate the applicability of the proposed aptasensor, nine human serum samples from Xinyang Central Hospital were measured by using the proposed aptasensor and ROCHE 72601 ECL method employed by Xinyang Central Hospital as the reference method. The results were listed in table 1. The results obtained via two different methods were in good agreement with the regression equation Y = 1.023 X - 0.1064 (X, the proposed method; Y, the reference method) and a correlation coefficient of 0.999. The statistical difference between the CEA concentrations measured by this method and ROCHE 72601 ECL method was examined by the two-sides F-test and t-test method (P = 0.95, the confidence level).

F-test method:

$$n_1 = 9,\ \overline{x_1} = 21.975,\ s_1 = 31.114$$
$$n_2 = 9,\ \overline{x_2} = 21.555,\ s_2 = 30.432$$
$$F = \frac{s_1^2}{s_2^2} = \frac{(31.114)^2}{(30.432)^2} = 1.05$$
$$F_{standard} = 3.44$$
$$F < F_{standard}$$

$\overline{x_1}$ and $\overline{x_2}$ are the average value of the CEA concentrations of nine samples measured by ROCHE 72601 ECL method and this ECL aptasensor method, respectively. The results showed that there is no significant difference between the two methods.

T-test method:

The pooled standard deviation can be calculated to be 30.773.

$$s = 30.773$$
$$t = \frac{|\overline{x_1} - \overline{x_2}|}{s}\sqrt{\frac{n_1 \times n_2}{n_1 + n_2}} = \frac{|21.975 - 21.555|}{30.773}\sqrt{\frac{9 \times 9}{9 + 9}} = 0.03$$
$$As\ P = 0.95,\ f = n_1 + n_2 - 2 = 16$$
$$t_{0.95,16} = 2.09$$
$$t < t_{0.95,16}$$

Therefore, there is no significant difference between the two methods.

Here Table 1

To further evaluate the applicability of the aptasensor, the recovery experiments were performed by standard addition methods. As listed in table 2, the recoveries are in the range from 85.0 to 109.5%, the RSD values are less than 3.4%, indicating that the aptasensor had good accuracy and potential for the analysis of CEA in real clinical samples.

Here Table 2

4. Conclusion

In this work, a sensitive and selective label-free ECL aptasensor was developed for detection of CEA. The tripetalous structure CdS-GR nanocomposites were prepared via a simple one-step hydrothermal method and characterized by SEM, TEM, XRD, Raman, and FTIR. The prepared nanomaterials possess some excellent properties such as large specific surface area, high ECL intensity, and high stability. L-cys and AuNPs were used as signal amplifier to improve the sensitivity of the aptasensor. The proposed aptasensor has been applied to determination of CEA in the real human serums samples. With advantages such as simple preparation, convenient operation, high sensitivity and good selectivity, this strategy has the potential for biochemical applications.

Acknowledgments

This work was supported by the National Natural Science Foundation of China (21375114, U1304214), the Project of Science and Technology development of Henan Province (142300410197), and the Foundation of Henan Educational Committee (14A150013), and Foundation for Key Young Teachers from Xinyang Normal University (2014GGJS-05).

References

1 A. B. Iliuk, L. Hu and W. A. Tao, *Anal. Chem.*, 2011, **83**, 4440-4452.

2 M. R. Parkhurst, J. C. Yang, R. C. Langan, M. E. Dudley, D. A. Nathan, S. A. Feldman, J. L. Davis, R. A. Morgan, M. J. Merino, R. M. Sherry, M. S. Hughes, U. S. Kammula, G. Q. Phan, R. M. Lim, S. A. Wank, N. P. Restifo, P. F. Robbins, C. M. Laurencot and S. A. Rosenberg, *J. Am. Chem. Soc.*, 2011, **19**, 620-626.

3 G. R. H. Tabar and C. L. Smith, *World App. Sci.J.*, 2010, **8**, 16-21.

4 X. X. Zeng, S. S. Ma, J. C. Bao, W. W. Tu and Z. H. Dai, *Anal. Chem.*, 2013, **85**, 11720-11724.

5 Z. B. Huang, X. Zhou, J. Xu, Y. P. Du, W. Zhu, J. Wang, Y. Q. Shu and P. Liu, *J. Clin. Oncol.*, 2014, **5**, 170-176.

6 F. Y. Kong, Z. Xu, M. T. Xu, J. J. Xu and H. Y. Chen, *Electrochim, Acta*, 2011, **56**, 9386-9390.

7 K. J. Huang, D. J. Niu, W. Z. Xie and W. Wang, *Anal. Chim. Acta*, 2010, **659**, 102-108.

8 S. Y. Deng and H. X. Ju, *Analyst*, 2013, **138**, 43-61.

9 J. Kim, S. Y. Kwon, J. K. Park and I. K. Park, *Biosens. Bioelectron.*, 2014, **55**, 209-215.

10 Y. M. Liu, H. Y. Yue, W. Tian, Y. H. Chen and F. R. Li, *Anal. Lett.*, 2009, **42**, 45-57.

11 Z. M. Zhou, J. Zhou, J. Chen, R. N. Yu, M. Z. Zhang, J. T. Song and Y. D. Zhao,

Biosens. Bioelectron., 2014, **59**, 397-403.

12 Z. Y. Lin, G. Y. Zhang, W. Q.Yang, B. Qiu and G. N. Chen, *Chem. Commun.*, 2012, **48**, 9918-9920.

13 H. W. Shu, W. Wen, H. Y. Xiong, X. Y. Zhang and S. F. Wang, *Electrochem. Commun.*, 2013, **37**, 15-19.

14 Y. Q. Dong, C. Q. Chen, J. P. Lin, N. N. Zhou, Y. W. Chi and G. N. Chen, *Carbon.*, 2013, **56**, 12-17.

15 H. T. Xiong and X. W. Zheng, *Analyst*, 2014, **139**, 1732-1739.

16 Z. F. Ding, B. M. Quinn, S. K. Haram, L. E. Pell, B. A. Korgel and A. J. Bard, *Science*, 2002, **296**, 1293-1297.

17 L. Deng, Y. Shan, J. J. Xu and H. Y. Chen, *Nanoscale*, 2012, **4**, 831-836.

18 J. P. Feser, E. M. Chan, A. Majumdar, R. A. Segalman and J. J. Urban, *Nano Lett.*, 2013, **13**, 2122-2127.

19 M. G Panthani., J. M. Kurley, R. W. Crisp, T. C. Dietz, T. Ezzyat, J. M. Luther and D. V. Talapin, *Nano Lett.*, 2014, **14**, 670-675.

20 A. H. Ye, W. Q. Fan, Q. H. Zhang, W. P. Deng and Y. Wang, *Catal. Sci. Technol.*, 2012, **2**, 969-978.

21 S. Q. Liu, M. Q. Yang and Y. J. Xu, *J. Mater. Chem.*, 2014, **2**, 430-440.

22 P. Gao, J. C. Liu, D. D. Sun and D. Delai, *J. Hazard. Mater.*, 2013, **250**, 412-420.

23 J. G. Yu, J. Jin, B. Cheng and M. Jaroniec, *J. Mater. Chem.*, 2014, **2**, 3407-3416.

24 A. Schinwald, F. Murphy, A. Askounis, V. Koutsos, K. Sefiane, K. Donaldson and

C. J. Campbell, *Nanotoxicology*, 2014, **8**, 824-832.

25 Y. F. Yang, M. Li, Y. L. Xie, X. H. Song, X. W. Qu, H. Y. Zhao, *Mater. Lett.*, 2014, **118**, 184-187.

26 H. Zhou, Y. Y. Zhang, J. Liu, J. J. Xu and H. Y. Chen, *Chem. Commun.*, 2013, **49**, 2246-2248.

27 Q. Li, B. D. Guo, J. G. Yu, J. R. Ran, B. H. Zhang, H. J. Yan and J. R. Gong, *J. Am. Chem. Soc.*, 2011, **133**, 10878-10884.

28 Y. Shan, J. J. Xu and H. Y. Chen, *Nanoscale*, 2011, **3**, 2916-1923.

29 J. I. Cutler,; E. Auyeung and C. A. Mirkin, *J. Am. Chem. Soc.*, 2012, **134**, 1376-1391.

30 N. Xia, L. P. Zhang, G. F. Wang, Q. Q. Feng and L. Lin, *Biosens. Bioelectron.*, 2013, **47**, 461-466.

31 Y. Zhuo, G. F. Gui, Y. Q. Chai, N. Liao, K. Xiao and R. Yuan, *Biosens. Bioelectron.*, 2014, **53**, 459-464.

32 F. Lisdat, D. Schaefer and A. Kapp, *Anal. Bioanal. Chem.*, 2013, **405**, 3739-3752.

33 W. S. Hummers Jr and R. E. Offeman, *J Am Chem Soc.*, 1958, **80**, 1339-1339.

34 Z. Y. Gao, N. Liu, D. P. Wu, W. G. Tao, F. Xu and K. Jiang, *Appl. Surf. Sci.*, 2012, **258**, 2473-2478.

35 G. Frens, *Nature*, 1973, **241**, 20-22.

36 Y. Hu, X. H. Gao, L. Yu, Y. R. Wang, J. Q. Ning, S. J. Xu and X. W. Lou, *Angew. Chem. Int. Edit.*, 2013, **52**, 5636-5639.

37 W. J. Han, L. Ren, X. Qi, Y. D. Liu, X. L. Wei, Z. Y. Huang, J. X. Zhong, *Appl. Surf. Sci.*, 2014, **299**, 12-18.

38 X. M. Zhao, S. W. Zhou, L. P. Jiang, W. H. Hou, Q. M. Shen and J. J. Zhu. *Chem. Eur. J.*, 2012, **18**, 4974-4981.

39 J. H. Wang, S. Liang, L. Ma, S. J. Ding, X. F. Yu, L. Zhou, Q. Q. Wang, *CrystEngComm.*, 2014, **16**, 399-405.

Table 1

Analytical results of the proposed ECL aptasensor and ROCHE ECL method for CEA in human serum samples.

Serum sample	ROCHE ECL method (ng/mL)	This work (ng/mL)	Relative errors (%)
1	62.57	60.58	-3.2
2	31.17	30.16	-3.2
3	11.98	12.14	1.3
4	83.93	82.74	- 1.4
5	0.855	0.896	4.8
6	2.50	2.769	10.8
7	1.84	1.811	-1.6
8	2.41	2.363	-9.1
9	0.524	0.539	2.9

Serum samples 1-4 and 5-9 were diluted with PBS at 10 and 0 times, respectively.

Table 2 Recovery test for CEA in spiked human serum.

Found (ng/mL)	Added (ng/mL)	Total found (ng/mL)	Recovery (%)	RSD (%, n = 3)
2.363	0.05	2.409	92.0	1.5
2.363	0.50	2.872	101.8	3.4
2.363	5.0	7.261	98.0	2.6
0.896	0.02	0.913	85.0	1.3
0.896	0.20	1.115	109.5	2.1
0.896	2.0	2.95	102.7	1.7

Figure captions

Scheme 1. The schematic representation of the fabrication process for ECL aptasensor.

Fig. 1. SEM images of GO (A), GR (B), CdS (C) and CdS-GR (D).

Fig. 2. TEM images of GR (A), CdS (B) and CdS-GR (C).

Fig. 3. (A) Raman spectra of (a) GR, (b) CdS-GR and (c) CdS nanocomposites. (B) XRD patterns of (a) GO, (b) GR, (c) CdS, and (d) GR–CdS nanocomposites and (C) FT-IR spectra.

Fig. 4. EIS (A) and ECL (B) behaviors of bare GCE (a), CdS-GR/GCE (b), nafion/CdS-GR/GCE (c), L-cys/nafion/CdS-GR/GCE (d), AuNPs/L-cys/nafion/CdS-GR/GCE (e), Aptamer/AuNPs/L-cys/nafion/CdS-GR /GCE (f), BSA/Aptamer/AuNPs/L-cys/nafion/CdS-GR/GCE/GCE (g) and CEA/BSA/Aptamer/AuNPs/L-cys/nafion/CdS-GR/GCE (h). EIS in 5 mM $Fe(CN)_6^{3-}/Fe(CN)_6^{4-}$ (1:1) containing 0.1 M KCl. ECL working solution was 0.1 M pH 7.4 PBS containing 0.1 M KCl and 0.1 M $K_2S_2O_8$. The CVs proceeded between 0 to -1.6 V with a scan rate of 100 mV s^{-1}.

Fig. 5. Effects of pH of detect solution (A), concentration of KCl (B) and $K_2S_2O_8$ (C), and the incubation time (D) on the ECL intensity.

Fig. 6. The ECL intensity-time curve (A) and calibration curve (B) of various concentrations of CEA: a–k: 0, 0.01, 0.05, 0.1, 0.25, 1.0, 2.5, 5.0, 10.0, 20.0 ng/mL. Other conditions are the same as Fig. 4B.

Fig. 7. Selectivity (A) and stability (B) of the ECL aptasensor. The concentrations of HSA, hIgE, hIgG, and CEA are 40 mg/mL, 20 mg/mL, 20 mg/mL, 1.0 ng/mL, respectively. Other conditions are the same as Fig. 4B.

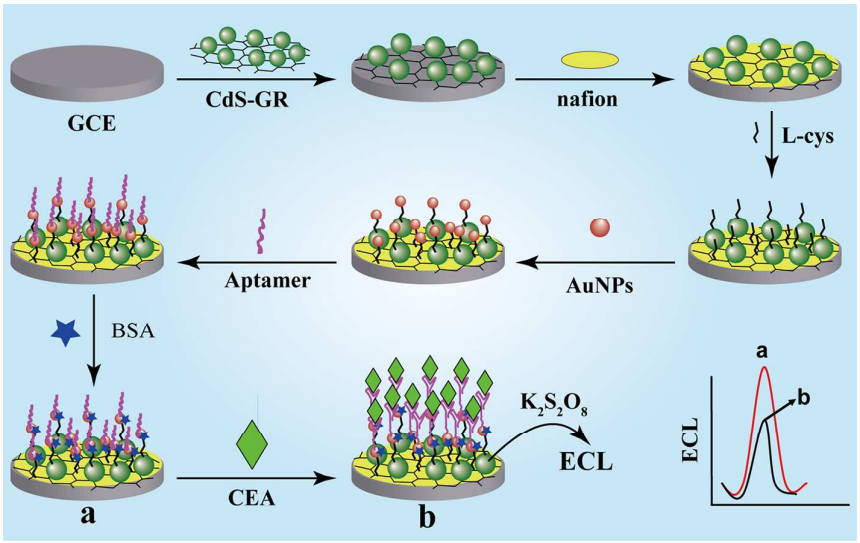

Scheme 1

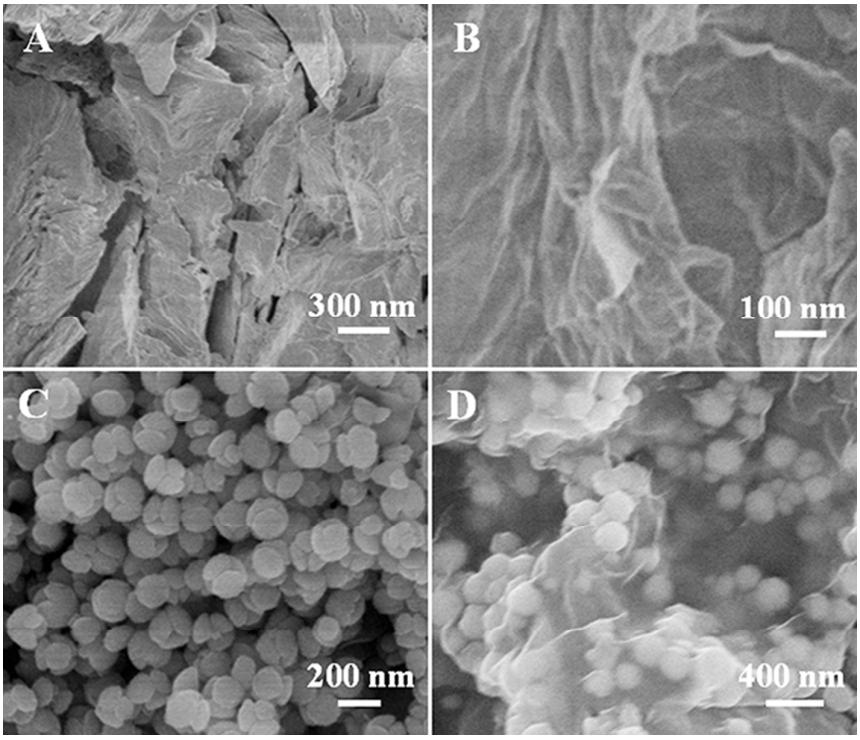

Fig. 1

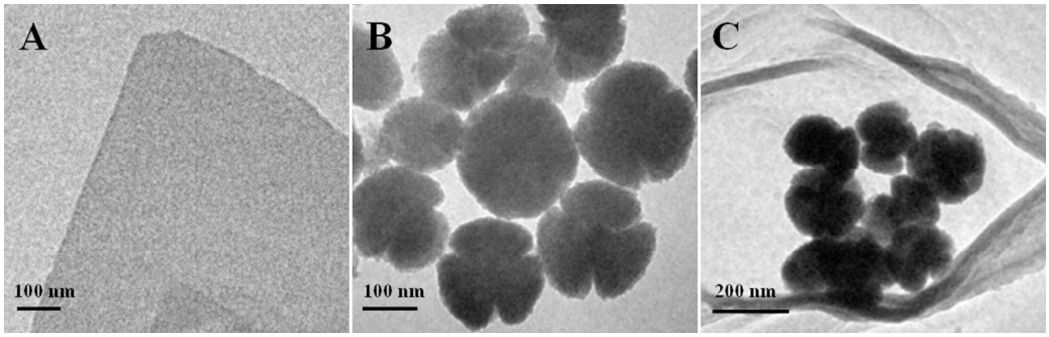

Fig. 2

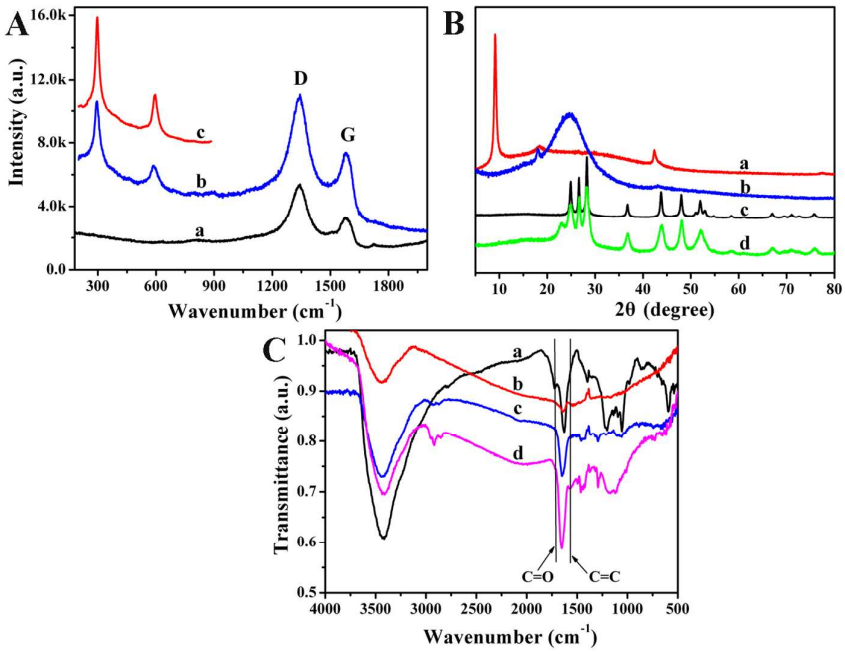

Fig. 3

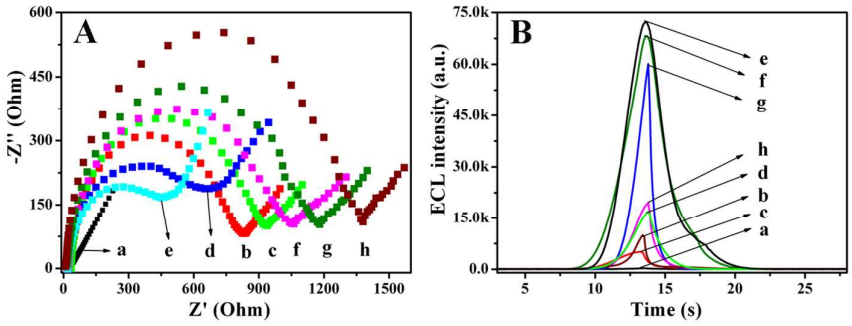

Fig. 4

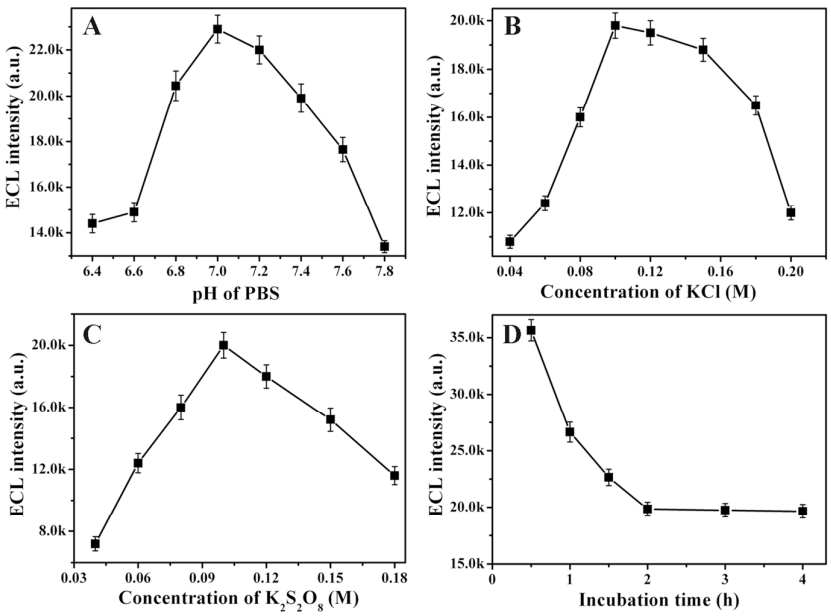

Fig. 5

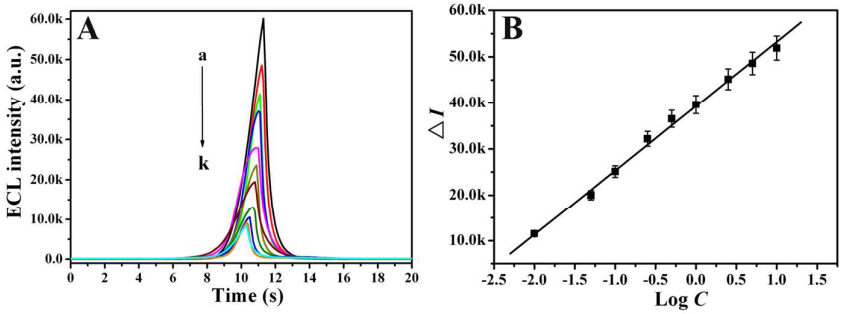

Fig. 6

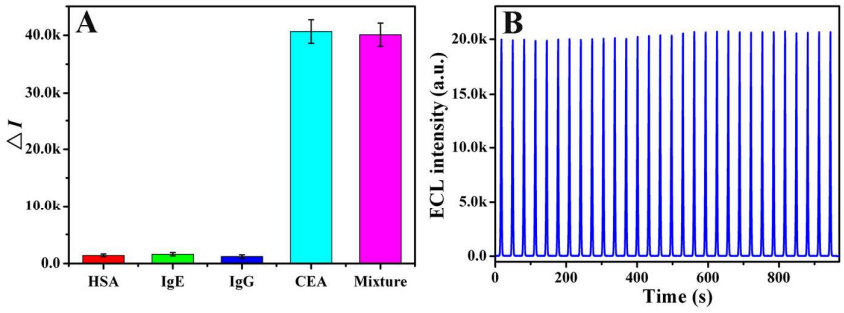

Fig. 7

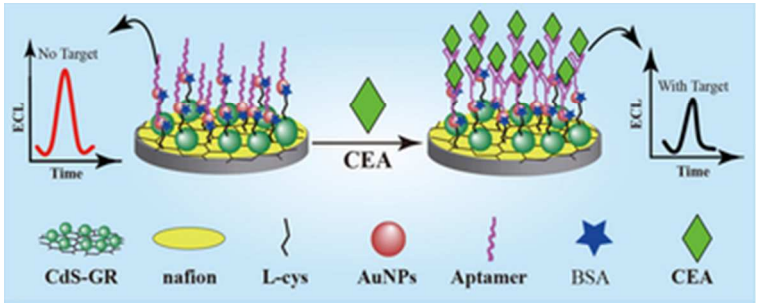

31x12mm (300 x 300 DPI)